photonics

MDPI

Article

The Super Phase Sensitivity of an SU(1,1) Interferometer with a Two-Mode Squeezed Coherent State via Balanced Homodyne and Intensity Detection

Changlan Xu [1], Lei Wang [1], Shaoqiu Ke [1], Jun Liu [1,*] and Dongxu Chen [2]

[1] School of Science, Jiangsu University of Science and Technology, Zhenjiang 212003, China
[2] Quantum Information Research Center, Shangrao Normal University, Shangrao 334001, China
* Correspondence: junliu@just.edu.cn

Abstract

We propose a novel scheme that is used for the enhancement of phase sensitivity. The SU(1,1) interferometer with a two-mode squeezed coherent state input, using balanced homodyne detection (BHD) and intensity detection (ID), is shown. Our results demonstrate that the phase sensitivity achieved via BHD outperforms that of ID. The optimal phase sensitivity via BHD surpasses the Heisenberg limit (HL) and approaches the quantum Cramér–Rao bound. A larger photon number and parameter strength can make the phase sensitivity better. Furthermore, we show the effects of internal and external losses on phase sensitivity in detail. When external loss reaches 10%, the phase sensitivity can reach the HL. Next, we have a detailed discussion on the impact of the squeezing parameter and photon number on phase sensitivity, which shows that our scheme has better phase sensitivity and enhanced robustness. This interferometer system thus holds significant potential for applications in quantum precision measurement.

Keywords: phase sensitivity; SU(1,1) interferometer; two-mode squeezed coherent state; hybrid interferometer

1. Introduction

Quantum technology and quantum information have received significant attention and witnessed substantial developments in recent decades [1,2]. Quantum metrology, as a part of quantum technology, has drawn much attention and been applied extensively in numerous practical domains [3–6]. The purpose of quantum metrology is to enhance measurement precision. Usually, optical interferometers are utilized to improve phase measurement precision [7]. One typical optical interferometer is the Mach–Zehnder interferometer (MZI), which is a type of linear interferometer described by the SU(2) group [8]. It consists of two beam splitters (BSs) and a phase shifter. The BSs play an important role in the measurement process. The first BS is used to split the beam, while the other one integrates two beams after propagating on different paths. The phase sensitivity is limited to $\frac{1}{\sqrt{N_L}}$, where N_L is the input photon number in the MZI. $\frac{1}{\sqrt{N_L}}$ is named as shot noise limit (SNL) or standard quantum limit. In order to obtain the better phase sensitivity, many quantum states have been proposed, such as the N00N state [9,10], two-mode squeezed vacuum state [11], entangled coherent state [12] and Fock state [13]. However, these quantum states have many drawbacks. For the N00N state, its photon number is extremely low and it is also very sensitive to losses. Without the boost of the coherent

Received: 4 February 2026
Revised: 11 March 2026
Accepted: 19 March 2026
Published: 23 March 2026

state, the total photon number of the two-mode squeezed vacuum state is also very small. Moreover, the squeezing degree of the current experiment technology cannot surpass 20 dB [14–16]. Therefore, to achieve the practical application of quantum metrology, more methods need to be employed.

A useful method is to modify the structure of the optical interferometer. A novel type of interferometer is named as an SU(1,1) interferometer because the transformation relationship is described by the SU(1,1) group, which was first proposed by Yurke et al. in 1986 [8]. Contrary to MZI, the SU(1,1) interferometer consists of positive nonlinear elements, such as an optical parametric amplifier (OPA) and four-wave mixing (FWM) [17,18]. The input beams experience the first OPA, and the photon number inside the SU(1,1) interferometer will be increased due to the amplification of the OPA [19,20]. Then, one of the beams undergoes a phase shift and carries the phase information. For the phase sensitivity measurement, Li et al. proposed that the phase sensitivity can approach the Heisenberg limit (HL) with the input of a coherent state and the squeezed vacuum state by balanced homodyne detection (BHD) [21]. Ou et al. pointed out that with the input of the vacuum state the phase sensitivity can also reach the HL [22]. The HL is defined as $\Delta\phi_{\mathrm{HL}} = \frac{1}{N_{\mathrm{H}}}$, where N_{H} is the total photon number inside the SU(1,1) interferometer.

Meanwhile, a modified SU(1,1) interferometer is proposed by Zhang et al. [23]. It has the advantage of a simple structure and high precision phase sensitivity. The modified SU(1,1) interferometer, which is also named as the hybrid interferometer (HI), has been investigated by many groups [24,25]. Nevertheless, when the intensities of the two arms are different, it will lead to a decrease in phase sensitivity. And the optimal phase sensitivity can be achieved with different transmissivities of the BS when the squeezing parameter is changed. Therefore, more groups have focused on the SU(1,1) interferometer [26,27]. By adjusting the parameter ratio of the two OPAs, super phase sensitivity can still be achieved with detection losses as high as 80% [26]. By performing non-Gaussian operations in two arms of an SU(1,1) interferometer, the phase sensitivity is further improved, and the photon losses are also effectively reduced [27].

In addition to a different structure for the optical interferometer, another method to have better phase sensitivity is to employ different detection methods, such as intensity detection (ID), BHD and parity detection. ID has the advantage of a simple structure [28]. BHD has been widely employed in phase sensitivity measurement, such as in LIGO [7]. With the employment of parity detection, the phase sensitivity can reach the HL when the input is a two-mode squeezed vacuum state [11]. Therefore, all possible methods need to be employed to have the optimal phase sensitivity. Nevertheless, considering endless detection methods is impractical. Fortunately, this challenge can be effectively tackled by employing quantum Fisher information (QFI) and quantum Cramér–Rao bounds (QCRB), $\Delta\phi^2_{\mathrm{QCRB}} = \frac{1}{F}$ [19,29,30]. Jarzyna et al. discussed the QFI of MZI when the phase shifter is placed in two arms [31]. Lang and Caves also proposed a two-parameter estimation of QFI for MZI [32]. Ataman and Preda considered single QFI and double QFI with the same input [33].

Recently, QFI with a two-mode squeezed coherent state based on the HI has been proposed and can be utilized for the improvement of phase sensitivity [24]. The photon number of the two-mode squeezed coherent state can be large enough due to the boost of the coherent state. However, the transmissivity of the BS in the HI needs to be dynamic when the squeezing parameter of the FWM is different. Additionally, only the degenerate FWM can be applied in the HI. For these reasons, instead of using the HI scheme, in this paper we investigate the phase sensitivity by combining the use of the SU(1,1) interferometer with an input represented by a two-mode squeezed coherent state. Meanwhile, considering that the effect of photon losses is inevitable in the measurement process, we analyze the phase sensitivity in detail under ideal and photon loss conditions.

This paper is structured as follows: In Section 2, the scheme employing a two-mode squeezed coherent state as the input of an SU(1,1) interferometer is introduced. In Section 3, we calculate the QFI, SNL and HL. In Section 4, we analyze the phase sensitivity via BHD and ID. In Section 5, the effects of photon losses in the scheme are shown. In Section 6, we have a detailed discussion on the phase sensitivity and robustness. The conclusion is drawn in the last section.

2. Model

The structure of an SU(1,1) interferometer is shown in the Figure 1, which contains three FWMs and a phase shifter. A coherent beam and a vacuum beam enter the FWM1, which is used to generate a two-mode squeezed coherent state. It is a phase insensitive process [34]. Then, the two output beams are injected into the SU(1,1) interferometer, which consists of the FWM2 and the FWM3. Without the FWM1 process, this structure of an SU(1,1) interferometer will reduce to an ordinary SU(1,1) interferometer, which was experimentally realized in 2011 [35]. The phase sensitivity can reach sub-SNL. After the SU(1,1) interferometer, this beam will enter photon detection. The transformation of the FWM1 can be described as

$$\begin{aligned} \hat{a}_1 &= \sqrt{G_1}\hat{a}_0 + e^{i\theta_1}\sqrt{G_1-1}\hat{b}_0^\dagger, \\ \hat{b}_1 &= \sqrt{G_1}\hat{b}_0 + e^{i\theta_1}\sqrt{G_1-1}\hat{a}_0^\dagger, \end{aligned} \tag{1}$$

where G_1 and θ_1 are the gain and phase of the FWM1. $G_1 = \cosh^2 r_1$, r_1 is the parametric strength of FWM1. $\hat{a}_i(\hat{a}_i^\dagger)$ and $\hat{b}_i(\hat{b}_i^\dagger)$ $(i = 0, 1, 2, 3, 4)$ are annihilation (creation) operators of the mode A(B), respectively. As illustrated in Figure 1, the FWM process corresponds to a cyclic sequence: one pump photon is annihilated, a probe photon is generated, a second pump photon is annihilated, and a conjugate photon is subsequently created. The annihilation operators corresponding to the probe and the conjugate fields are designated as $\hat{a}$ and $\hat{b}$, respectively. The interaction Hamiltonian can be written as $\hat{H} = i\hbar\zeta e^{-i\theta}\hat{b}^\dagger\hat{a}^\dagger + \text{h.c.}$, where ζ denotes the interaction strength, which is proportional to the pump light intensity. Moreover, the parameter ζ exhibits a strong dependence on both the one-photon detuning Δ and the two-photon detuning δ. Usually, Δ is about 800 MHz and δ is around 4 MHz. Here, $\theta = 2\phi_{\text{pump}}$, where ϕ_{pump} stands for the phase of the pump field [34]. For the coherent beam, it has $\langle\hat{a}_0\rangle = |\alpha|e^{i\theta_\alpha}$. θ_α is the phase of the coherent state. α is the amplitude. $N = |\alpha|^2$, N is the photon number of the coherent state input. For the vacuum state, $\langle\hat{b}_0\rangle = |\beta|e^{i\theta_\beta}$, θ_β is the phase of the vacuum state. $|\beta| = 0$.

The transformation relationship of FWM2 process is

$$\begin{aligned} \hat{a}_2 &= \sqrt{G_2}\hat{a}_1 + e^{i\theta_2}\sqrt{G_2-1}\hat{b}_1^\dagger, \\ \hat{b}_2 &= \sqrt{G_2}\hat{b}_1 + e^{i\theta_2}\sqrt{G_2-1}\hat{a}_1^\dagger, \end{aligned} \tag{2}$$

where $G_2 = \cosh^2 r_2$ and θ_2 are the gain and phase of the FWM2 and r_2 is the parametric strength. The input photon number of the SU(1,1) interferometer can be expressed as $< \hat{N}_{in} >=< \hat{a}_1^\dagger\hat{a}_1 > + < \hat{b}_1^\dagger\hat{b}_1 >$. $N_{in} = (2G_1 - 1)N + 2(G_1 - 1)$. According to the transformation relationship, the photon number of the upper arm can be expressed as

$$\begin{aligned} N_u =& < \hat{a}_2^\dagger\hat{a}_2 > \\ &= [G_1G_2 + (G_1-1)(G_2-1)]N \\ &+ 2\sqrt{G_1G_2(G_1-1)(G_2-1)}\cos(\theta_1-\theta_2)(N+1) \\ &+ [G_2(G_1-1) + G_1(G_2-1)]. \end{aligned} \tag{3}$$

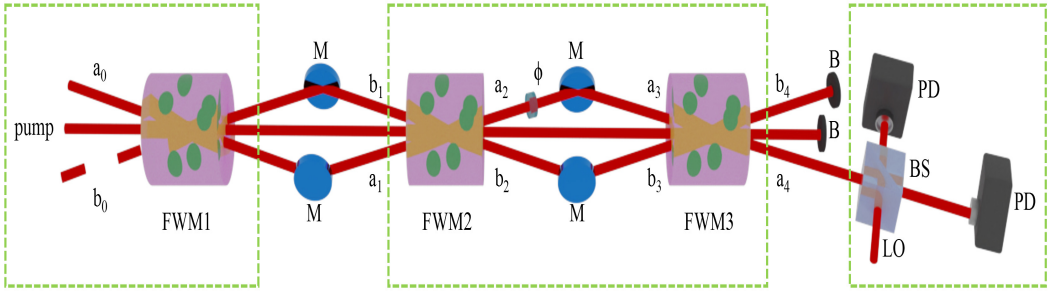

Figure 1. Diagrammatic sketch of an SU(1,1) interferometer for phase sensitivity measurement. It can be divided into three sections. For the first part, it is the state generation. An SU(1,1) interferometer, which contains the FWM2 and FWM3, is placed in the second part. The last part shows the detection process. The red dashed line represents a vacuum beam. M: mirror, ϕ: phase shifter, PD: photon detection, LO: the local beam, FWM: four-wave mixing. The LO is prepared for balanced homodyne detection.

The photon number of the lower arm can be expressed as

$$\begin{aligned} N_l =& < \hat{b}_2^\dagger \hat{b}_2 > \\ &= [G_2(G_1-1)+G_1(G_2-1)](N+1) \\ &+ 2\sqrt{G_1G_2(G_1-1)(G_2-1)}\cos(\theta_1-\theta_2)(N+1). \end{aligned} \tag{4}$$

The total photon number inside the SU(1,1) interferometer is $N_H = N_u + N_l$.

$$\begin{aligned} N_H =& [G_1G_2+(G_1-1)(G_2-1)]N \\ &+ 4\sqrt{G_1G_2(G_1-1)(G_2-1)}\cos(\theta_1-\theta_2)(N+1) \\ &+ [G_2(G_1-1)+G_1(G_2-1)](N+2). \end{aligned} \tag{5}$$

Then, the SNL and HL can be defined as $\Delta\phi_{\mathrm{SNL}} = \frac{1}{\sqrt{N_H}}$ and $\Delta\phi_{\mathrm{HL}} = \frac{1}{N_H}$. Equation (5) shows that the larger gains G_1 and G_2 represent a higher photon number.

For our scheme, the total input-output relation after the FWM3 process can be written as $\hat{a}_4 = \sqrt{G_3}\hat{a}_3 + e^{i\theta_3}\sqrt{G_3-1}\hat{b}_3^\dagger$. For simplifying, we assume that $\theta_1 = \theta_2 = \theta_3 = 0$ and $\theta_\alpha = \frac{\pi}{4}$. Combining Equations (1) and (2), the total input-output relation is as follows

$$\hat{a}_4^\dagger = A_1\hat{a}_0^\dagger + A_2\hat{b}_0, \tag{6}$$

where $A_1 = e^{-i\phi}(\sqrt{G_1}\sqrt{G_2}\sqrt{G_3} + \sqrt{G_3}\sqrt{G_1-1}\sqrt{G_2-1}) + \sqrt{G_2}\sqrt{G_1-1}\sqrt{G_3-1} + \sqrt{G_1}\sqrt{G_2-1}\sqrt{G_3-1}$, and $A_2 = e^{-i\phi}(\sqrt{G_2}\sqrt{G_3}\sqrt{G_1-1} + \sqrt{G_1}\sqrt{G_3}\sqrt{G_2-1}) + \sqrt{G_1}\sqrt{G_2}\sqrt{G_3-1} + \sqrt{G_1-1}\sqrt{G_2-1}\sqrt{G_3-1}$.

3. Quantum Cramér–Rao Bounds

As a powerful tool, QFI is employed to estimate the optimal value of unknown parameters [36], and it is irrelevant to specific measurement methods [18]. It contains the maximum amount of information about the unknown phase shift ϕ, indicating the lower bound of the QCRB, that is $\Delta\phi_{\mathrm{QCRB}} \geq \frac{1}{\sqrt{F}}$. In this section, a single QFI is calculated. Here, the unitary operator $\hat{U}_\phi = \mathrm{e}^{\mathrm{i}\hat{H}\phi}$, where $\hat{H} = \hat{a}_2^\dagger\hat{a}_2$ is the photon number operator on mode a. In the absence of losses, for the pure state, the corresponding QFI can be calculated as [18,37]

$$F = 4\mathrm{Re}(\langle\partial_\phi\psi_\phi|\partial_\phi\psi_\phi\rangle - |\langle\partial_\phi\psi_\phi|\psi_\phi\rangle|^2), \tag{7}$$

where $|\partial_\phi \psi_\phi\rangle = \partial|\psi_\phi\rangle/\partial\phi$, and $|\psi_\phi\rangle = \hat{U}_\phi \hat{S}_{\mathrm{OPA}_2}|\psi_{in}\rangle$. $|\psi_\phi\rangle$ is the state after passing through the phase shifter. The notation Re means the real-part. The state $|\psi_{in}\rangle$ is the input state of the FWM2, where $|\psi_{\mathrm{in}}\rangle = \hat{S}_{\mathrm{OPA}_1}(\zeta_1)\hat{D}(\alpha)|0_\mathrm{a}, 0_\mathrm{b}\rangle$. $|0_\mathrm{a}, 0_\mathrm{b}\rangle$ represents the two-mode vacuum state. $\hat{D}(\alpha)$ is the displacement operator. The $\hat{S}_{\mathrm{OPA}_1}(\zeta_1)$ is the two-mode squeezing operator defined as $\hat{S}_{\mathrm{OPA}_1}(\zeta_1) = e^{\zeta_1^* \hat{a}_0 \hat{b}_0 - \zeta_1 \hat{a}_0^\dagger \hat{b}_0^\dagger}$, with $\zeta_1 = r_1 e^{i\theta_1}$. The operator $\hat{S}_{\mathrm{OPA}_2}$ is expressed as $\hat{S}_{\mathrm{OPA}_2}(\zeta_2) = e^{\zeta_2^* \hat{a}_1 \hat{b}_1 - \zeta_2 \hat{a}_1^\dagger \hat{b}_1^\dagger}$, with $\zeta_2 = r_2 e^{i\theta_2}$. The QFI is calculated using Equation (7) and it is

$$\begin{aligned} F &= 4\langle \Delta^2 \hat{H} \rangle \\ &= 4[sN + n(N+1)], \end{aligned} \tag{8}$$

where the coefficient is $n = 8G_1^2G_2^2 - 8G_1^2G_2 - 8G_2^2G_1 + 8G_1G_2 + G_1^2 + G_2^2 - G_1 - G_2 + 2\sqrt{G_1(G_1-1)}\sqrt{G_2(G_2-1)}(4G_1G_2 - 2G_2 - 2G_1 + 1)$, and $s = n + 2G_1G_2 - G_1 - G_2 + 1 + 2\sqrt{G_1(G_1-1)}\sqrt{G_2(G_2-1)}$. Then, the QCRB is $\Delta\phi_{\mathrm{QCRB}} = \frac{1}{\sqrt{F}}$.

To investigate the impact of the unbalanced input state on QCRB, we introduce the photon number difference η, defined by $\eta = N_H - N_{in}$ ($\eta \neq 0$). The total photon number inside the SU(1,1) interferometer is significantly enhanced due to the squeezing effect of the FWM, which leads to a further improvement in the precision bound. We present the photon number difference η to analyze the relationships among the QCRB, the SNL, and the HL. A lower phase value implies superior phase sensitivity. As Figure 2a shows, the QCRB can surpass the HL when $\eta < 2.78$. With the increase of η, the QCRB, which represents an optimal theoretical precision, can be restricted to the sub-SNL. Additionally, the effects of r_1, r_2 and N on phase sensitivity $\Delta\phi_{\mathrm{QCRB}}$ are also extremely significant. We set r_1 as a fixed value to investigate the variation of $\Delta\phi_{\mathrm{QCRB}}$ with respect to r_2 and N. In Figure 2b, three scenarios are considered where $r_2 < r_1$, $r_2 = r_1$ and $r_2 > r_1$. With the increase in r_2, the phase sensitivity $\Delta\phi_{\mathrm{QCRB}}$ improves—this is due to the enhancement of the total photon number N_H. As the photon number N increases, the $\Delta\phi_{\mathrm{QCRB}}$ is improved. However, the optimal phase sensitivity is achieved when both r_2 and N are in the high-value range and $\Delta\phi_{\mathrm{QCRB}}$ approaches a constant value.

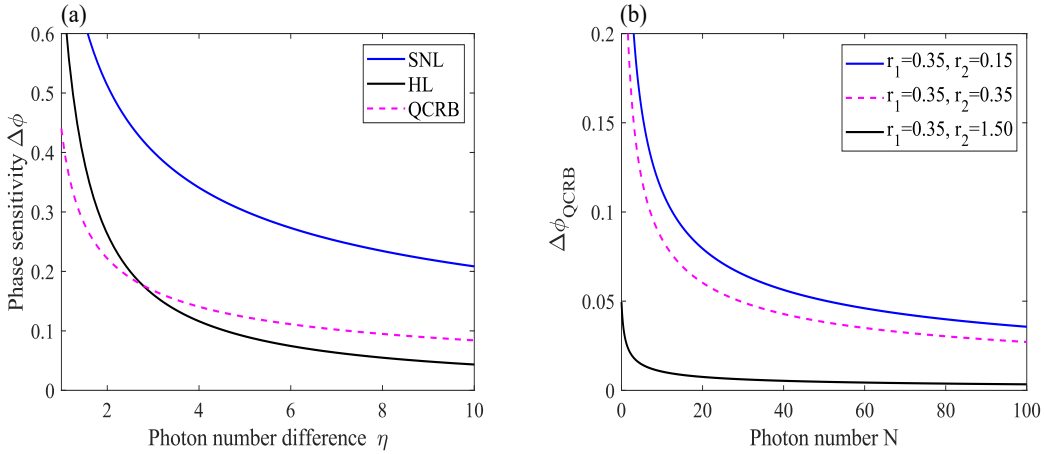

Figure 2. (**a**) QCRB versus photon number difference η. Compared with SNL and HL, here, $r_1 = r_2 = 0.35$. (**b**) QCRB versus photon number N with different squeeze parameters r_2. $\eta = N_H - N_{in}$ denotes the difference in photon number between that inside the interferometer and the input state. N represents the photon number of the coherent state. Here, $\Delta\phi_{\mathrm{SNL}} = \frac{1}{\sqrt{N_H}}$ and $\Delta\phi_{\mathrm{HL}} = \frac{1}{N_H}$.

4. Detection Methods

Next, we investigate the phase sensitivity of the SU(1,1) interferometer with different detection methods. The ID, as an ordinary detection method in the measurement process, is applied to measure the signal of the output port a. The detection operator in the scenario is given by

$$\begin{aligned}\hat{I} &= \hat{a}_{\text{out}}^{\dagger}\hat{a}_{\text{out}} \\ &= A_1A_3\hat{a}_0^{\dagger}\hat{a}_0 + A_1A_4\hat{a}_0^{\dagger}\hat{b}_0^{\dagger} + A_2A_3\hat{b}_0\hat{a}_0 + A_2A_4\hat{b}_0^{\dagger}\hat{b}_0 + A_2A_4.\end{aligned} \tag{9}$$

$A_1 = A_3^*$, $A_2 = A_4^*$. The slope of $\hat{I}$ is displayed as

$$\begin{aligned}\left|\frac{\partial\langle\hat{I}\rangle}{\partial\phi}\right| = |&2(2G_1-1)\sqrt{G_2(G_2-1)}\sqrt{G_3(G_3-1)}(N+1)\sin\phi \\ &+ 2(2G_2-1)\sqrt{G_1(G_1-1)}\sqrt{G_3(G_3-1)}(N+1)\sin\phi|.\end{aligned} \tag{10}$$

The variance is given by

$$\Delta^2\hat{I} = (2m^2+3m+1)N + m^2 + m, \tag{11}$$

where $m = 4G_1G_2G_3 - 2G_1G_2 - 2G_1G_3 - 2G_3G_2 + G_1 + G_2 + G_3 - 1 + 2(2G_3-1)\sqrt{G_1(G_1-1)}\sqrt{G_2(G_2-1)} + 2(2G_1-1)\sqrt{G_2(G_2-1)}\sqrt{G_3(G_3-1)}\cos\phi + 2(2G_2-1)\sqrt{G_1(G_1-1)}\sqrt{G_3(G_3-1)}\cos\phi$. According to the error-propagation formula, the phase sensitivity with ID can be calculated, which is

$$\begin{aligned}\Delta\phi &= \frac{\sqrt{\Delta^2\hat{I}}}{|\partial\langle\hat{I}\rangle/\partial\phi|} \\ &= \frac{\sqrt{(2m^2+3m+1)N+m^2+m}}{|2\sqrt{G_3(G_3-1)}(N+1)\sin\phi\left[(2G_1-1)\sqrt{G_2(G_2-1)}+(2G_2-1)\sqrt{G_1(G_1-1)}\right]|}.\end{aligned} \tag{12}$$

Additionally, BHD is applied in the SU(1,1) interferometer with the same input. In this scenario, the detection operator is given by

$$\begin{aligned}\hat{X} &= \hat{a}_{\text{out}} + \hat{a}_{\text{out}}^{\dagger} \\ &= A_1\hat{a}_0^{\dagger} + A_2\hat{b}_0 + A_3\hat{a}_0 + A_4\hat{b}_0^{\dagger}.\end{aligned} \tag{13}$$

The slope of $\hat{X}$ is displayed as

$$\begin{aligned}\left|\frac{\partial\langle\hat{X}\rangle}{\partial\phi}\right| = |&2\sqrt{N}\sqrt{G_1}\sqrt{G_2}\sqrt{G_3}\sin(\phi+\theta_\alpha) \\ &+ 2\sqrt{N}\sqrt{G_3}\sqrt{G_2-1}\sqrt{G_1-1}\sin(\phi+\theta_\alpha)|,\end{aligned} \tag{14}$$

and the variance is given by

$$\Delta^2\hat{X} = 2m+1. \tag{15}$$

The corresponding phase sensitivity can be obtained

$$\begin{aligned}\Delta\phi &= \frac{\sqrt{\Delta^2\hat{X}}}{|\partial\langle\hat{X}\rangle/\partial\phi|} \\ &= \frac{\sqrt{2m+1}}{|2\sqrt{N}\sin(\phi+\theta_\alpha)\left[\sqrt{G_1G_2G_3}+\sqrt{(G_1-1)(G_2-1)G_3)}\right]|}.\end{aligned} \tag{16}$$

In Figure 3, we compare the phase sensitivity of ID with that of BHD and consider its variation with the photon number N. In Figure 3a, the phase sensitivity with ID can only reach the sub-SNL. In contrast, for BHD, the optimal phase sensitivity can outperform the HL when ϕ is near π. Figure 3b illustrates the variation of phase sensitivity with photon number N. As the N increases, the phase sensitivity gradually improves. In the low-photon number region, both phase sensitivities can surpass the SNL. When N continues to increase, the phase sensitivity with BHD approaches the QCRB.

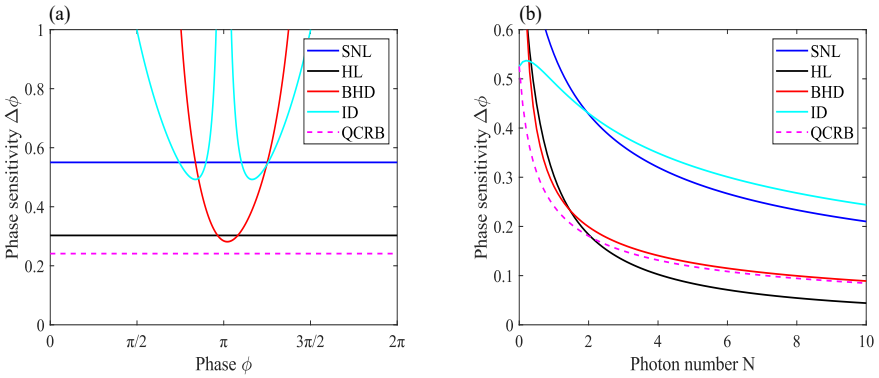

Figure 3. (**a**) The phase sensitivity is plotted against phase ϕ and compared with SNL, HL and QCRB with $N = 1$. (**b**) The phase sensitivity is plotted as a function of the photon number N. N represents the photon number of coherent state a. Here, $r_1 = r_2 = 0.35$ and $r_3 = 1.5$.

Furthermore, the effects of the squeezed parameters r_1, r_2 and r_3 on sensitivity have been displayed in Figure 4. The phase sensitivity with ID can beat the SNL when $0.24 < r_1 < 2.05$, as shown in Figure 4a. When $r_1 < 0.45$, the phase sensitivity with BHD can beat the HL. It is even worse than the SNL when $r_1 > 2.31$. With the increase in r_1, the phase sensitivity with ID gradually approaches the phase sensitivity with BHD. The QCRB also degrades to the HL. In Figure 4b, we obtain identical results due to the fact that FWM1 and FWM2 play the same role. If $r_1 = 0$, the SU(1,1) interferometer will become an ordinary SU(1,1) interferometer with the input of the coherent beam plus the vacuum beam [22]. Meanwhile, it is easy to find that it is also the ordinary SU(1,1) interferometer when $r_2 = 0$. In Figure 4c, the total photon number inside the SU(1,1) interferometer is related to the FWM1 and the FWM2. The SNL, HL and QCRB remain unchanged with the increase in r_3, as displayed in Figure 4c. The phase sensitivity with ID can reach the sub-SNL region when $r_3 > 1.11$ and the optimal phase sensitivity with BHD can surpass the HL when r_3 is larger than 0.87.

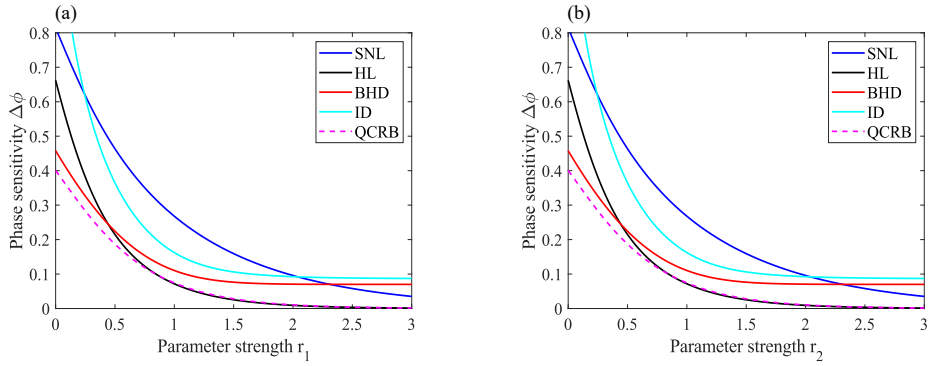

Figure 4. *Cont.*

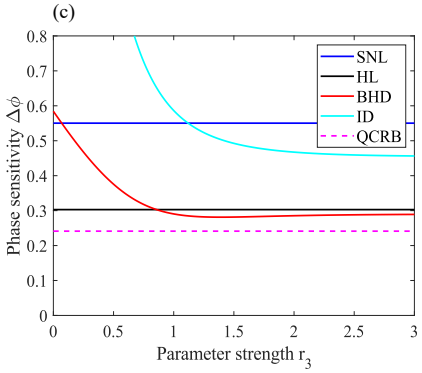

Figure 4. The phase sensitivity as a function of squeezing parameter strength, r_1 in (**a**), r_2 in (**b**) and r_3 in (**c**). Other parameters are $r_1 = r_2 = 0.35$, $r_3 = 1.5$ and $N = 1$. The rest are the same as those in Figure 3.

5. Losses on the Phase Sensitivity

In realistic scenarios, a variety of factors will reduce the phase sensitivity [22,38,39]. We focus on the impact of photon losses on the optimal phase sensitivity. The photon losses can be divided into two types: the internal loss and the external loss. In the experiments, the internal loss can be transmission loss inside the interferometer, and the external loss is due to the imperfect photon detector [40]. Here, the fictitious beam splitters 1 (FBS1) and FBS2 represent the internal loss and FBS3 represents the external loss in Figure 5.

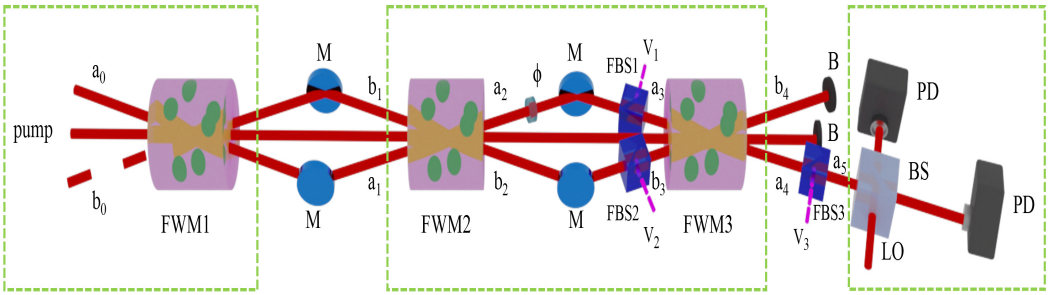

Figure 5. The scheme for phase sensitivity measurement with three fictitious beam splitters (FBSs). T_1, T_2 and T_3 are the transmissivities of the FBSs, respectively. The other conditions are the same as those in Figure 1.

The transmission of the FBS$_i$ (i = 1, 2, 3) is T_i, and the relationship of the FBSs can be shown as

$$\begin{aligned} \hat{a}_3 &= \sqrt{T_1} e^{i\phi} \hat{a}_2 + \sqrt{1 - T_1} \hat{v}_1, \\ \hat{b}_3 &= \sqrt{T_2} \hat{b}_2 + \sqrt{1 - T_2} \hat{v}_2, \\ \hat{a}_5 &= \sqrt{T_3} \hat{a}_4 + \sqrt{1 - T_3} \hat{v}_3. \end{aligned} \tag{17}$$

The phase sensitivities with ID and BHD are shown in Appendix A.

Figure 6 shows the phase sensitivity $\Delta\phi_{\text{loss}}$ with different transmissions T_i via ID and BHD. In Figure 6a,c,e, the phase sensitivity via ID is shown. It is not difficult to find that the phase sensitivity can reach the sub-SNL with $T_i = 1$, $r_1 = r_2 = 0.35$, $r_3 = 1.5$ and $N = 1$. Figure 6b,d,f show the phase sensitivity via BHD. Without the loss, the optimal phase sensitivity can reach the sub-HL. In Figure 6a, when T_1 is lower than 0.7, the phase sensitivity with ID is worse than the SNL. According to Figure 6c, the phase sensitivity is better than the SNL when the transmission T_2 is larger than 0.9. As Figure 6e shows, the phase sensitivity can reach the sub-SNL when the transmission T_3 is 0.5. In Figure 6b, we study the effect of T_1 on phase sensitivity with $T_2 = T_3 = 1$. The result indicates that

the phase sensitivity can reach the SNL when $T_1 = 0.5$. In Figure 6d, we study the effect of T_2 with $T_1 = T_3 = 1$. In this situation, the phase sensitivity is improved. It can beat the SNL when the loss is up to 0.5. As Figure 6f shows, better phase sensitivity can be achieved, and it can surpass the HL when the transmission T_3 reaches 0.9.

In Figure 7, we indicate the effects of the internal and external losses on the phase sensitivity. The phase sensitivity with BHD is better than that with ID when the loss is the same. In addition, for the phase sensitivity with BHD and ID, better phase sensitivity can be obtained by the larger transmission. For Figure 7a, with $T_1 = 0.1$ or $T_2 = 0.1$, increasing the transmission cannot improve the phase sensitivity. In the Figure 7b, the optimal phase sensitivity can be followed when T_1 is larger than 0.8. In Figure 7c,d, better phase sensitivity can be realized when T_1 and T_3 are larger. And they have the same trend. In Figure 7e, when $T_2 = 0.2$, increasing the transmission T_3 cannot boost the phase sensitivity. When T_2 is larger, the phase sensitivity is better. In Figure 7f, with $T_3 > 0.2$, increasing T_2 will lead to better phase sensitivity. When the transmissivity T_3 is 0.02, increasing the value of T_2 does not help in improving phase sensitivity.

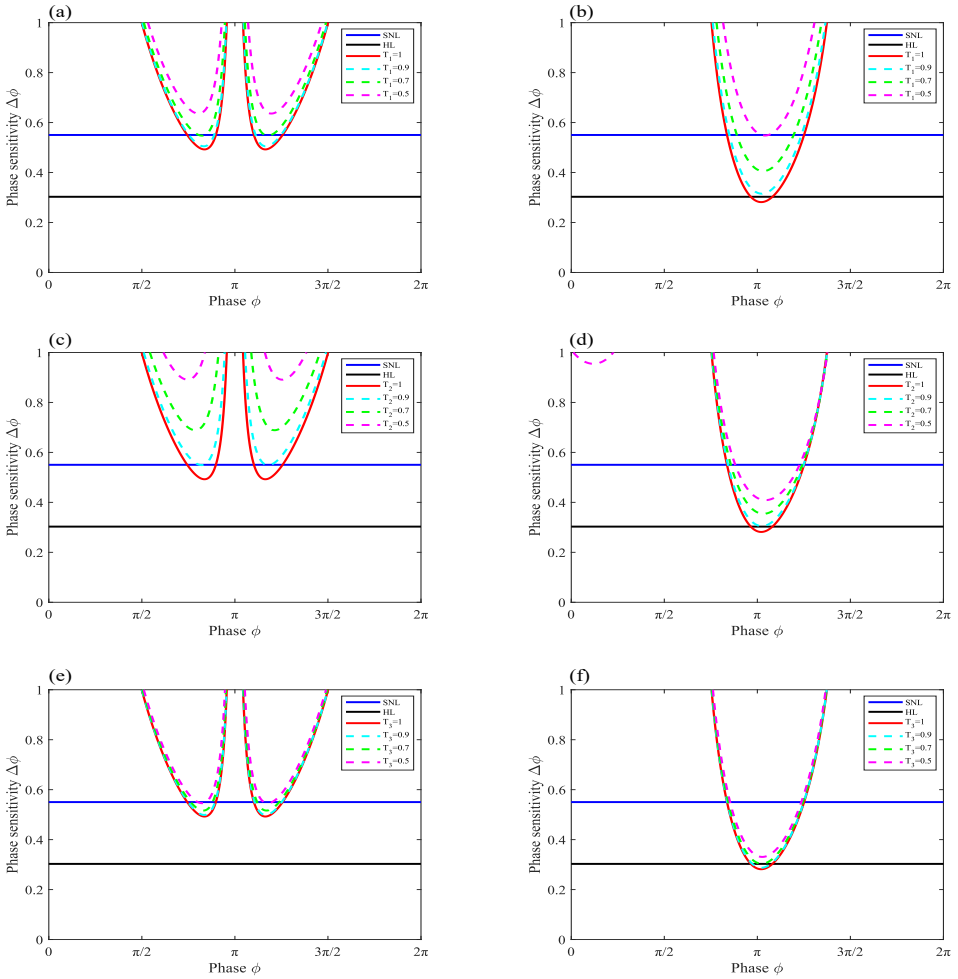

Figure 6. Phase sensitivity versus phase shift via ID in (**a**,**c**,**e**) and BHD in (**b**,**d**,**f**). The figure shows the phase sensitivity versus the phase shift with different transmissions T_1, T_2 and T_3. The other parameters are $r_1 = r_2 = 0.35$, $r_3 = 1.5$ and $N = 1$.

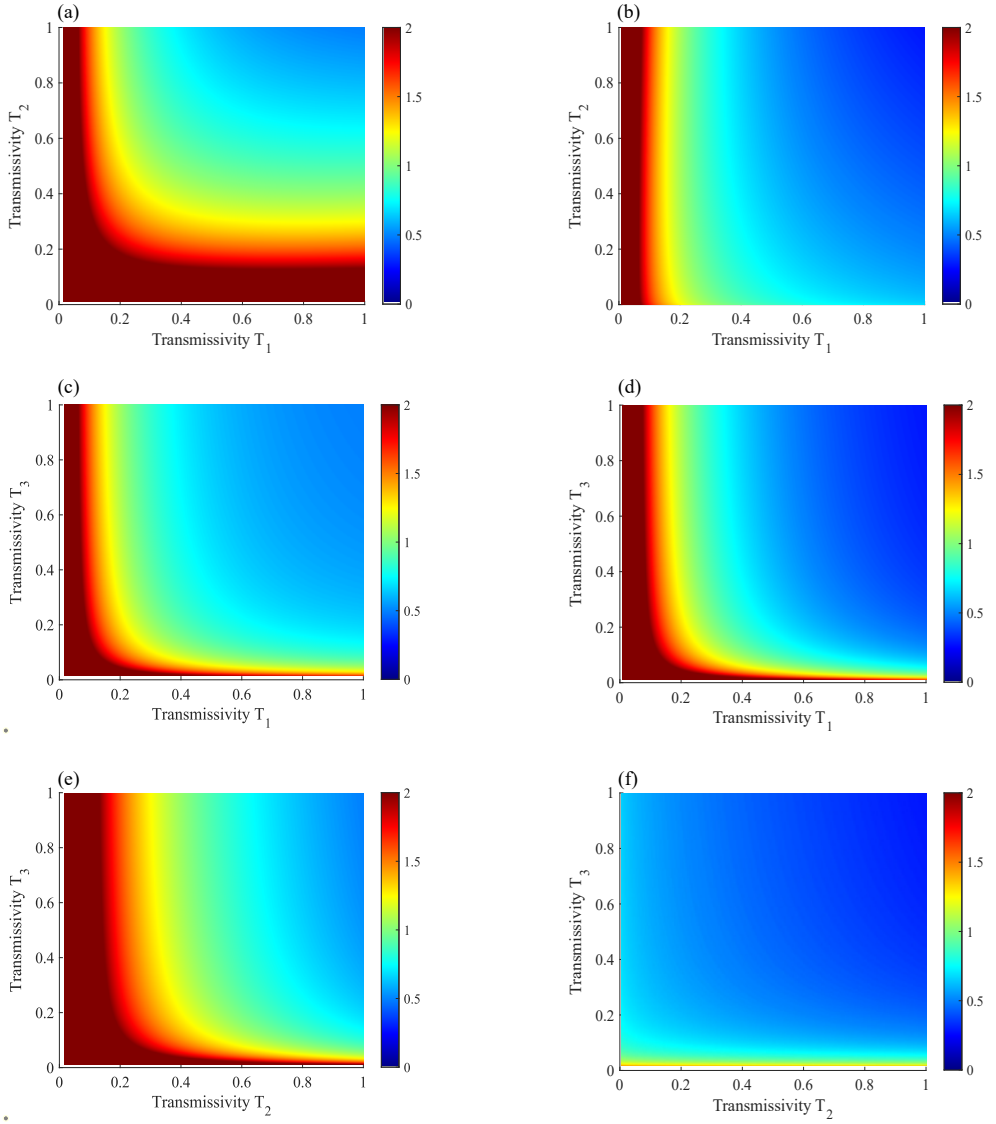

Figure 7. The phase sensitivity versus transmission via ID in (**a**,**c**,**e**) and BHD in (**b**,**d**,**f**). (**a**,**b**) shows the phase sensitivity versus T_1 and T_2 with $T_3 = 1$. (**c**,**d**) show the phase sensitivity versus T_1 and T_3 with $T_2 = 1$. (**e**,**f**) display the phase sensitivity versus T_2 and T_3 with $T_1 = 1$. The other parameters are the same as those in Figure 6.

In addition, to compare the robustness of the scheme with ID and BHD, Figure 8 is displayed. Here, the internal and external losses are the same ($T_i = 0.7, i = 1, 2, 3$). In Figure 8a, the phase sensitivities via BHD are always better than the SNL with increasing the photon number. And the phase sensitivity via ID is worse than the SNL. For Figure 8b,c, with the increase in the squeezing parameters r_1 and r_2, the phase sensitivity with BHD is better than that with ID. It can beat the SNL when $r_i > 1.12$ $(i = 1, 2)$. Meanwhile, the phase sensitivity with ID cannot surpass the SNL. According to Figure 8d, the phase sensitivity achieved via BHD can beat the SNL when r_3 is larger than 0.5. The phase sensitivity via ID is always worse than the SNL. In this case, the scheme with BHD has better robustness.

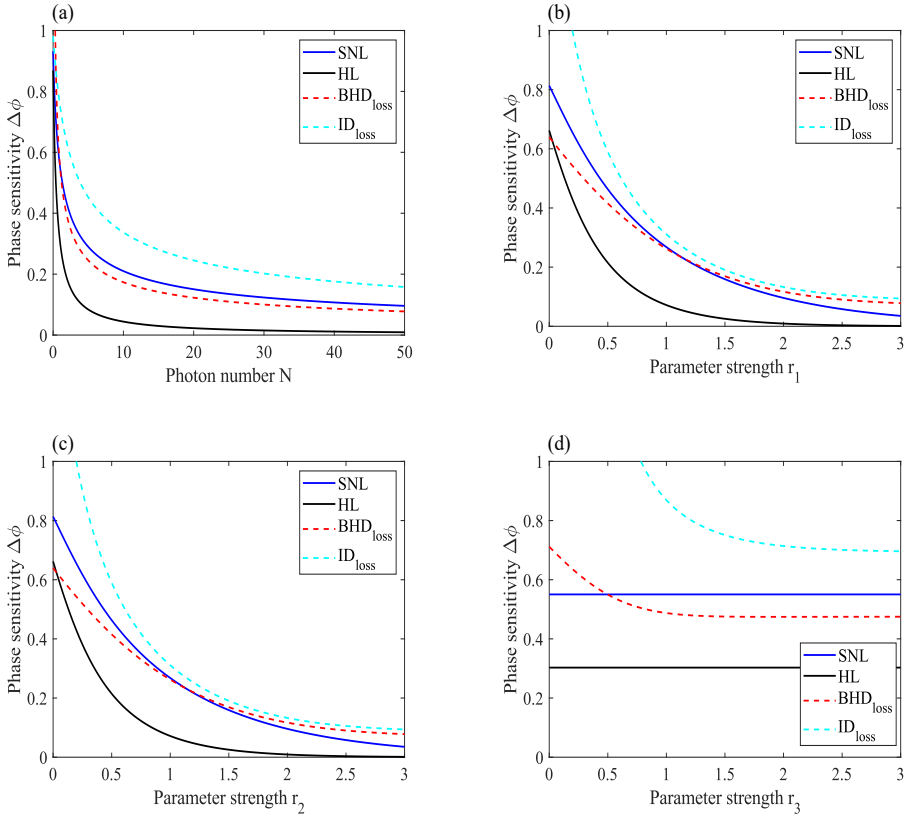

Figure 8. Phase sensitivity versus photon number in (**a**) and squeezing parameter strength r_i $(i = 1, 2, 3)$ in (**b**–**d**). Here, transmissivity T is set as $T_i = 0.7 (i = 1, 2, 3)$. The other parameters are the same as those in Figure 6.

6. Discussion

In this section, we have a detailed discussion that shows the advantage of our scheme. The HIs with the same input (two-mode squeezed coherent state) and the same detection method (BHD) are displayed in Figure 9 [24]. The structure in Figure 9 contains two FWMs and one BS. The total photon number inside the interferometer remains consistent with ours under the same parameters. This implies that the two schemes can obtain the same SNL and HL. According to the error-propagation formula, the phase sensitivity is

$$\Delta\phi = \frac{\sqrt{\Delta^2 \hat{H}_{\text{loss}}}}{|\partial\langle \hat{H}_{\text{loss}}\rangle/\partial\phi|}, \tag{18}$$

the variance is

$$\begin{aligned}\Delta^2 \hat{H}_{\text{loss}} = {} & \frac{1}{2}T_3(T_1+T_2)((2G_1-1)(2G_2-1)+4\sqrt{G_1G_2(G_1-1)(G_2-1)}) \\ & + 2T_3\sqrt{T_1T_2}((2G_1-1)\sqrt{G_2(G_2-1)}+(2G_2-1)\sqrt{G_1(G_1-1)})\cos\phi \\ & + \frac{1}{2}T_3(2-T_1-T_2)+(1-T_3),\end{aligned} \tag{19}$$

and the slope becomes

$$\left|\frac{\partial \hat{H}_{\text{loss}}}{\partial\phi}\right| = |\sqrt{2NT_1T_3}\left(\sqrt{(G_1-1)(G_2-1)}+\sqrt{G_1G_2}\right)\sin(\phi+\theta_a)|. \tag{20}$$

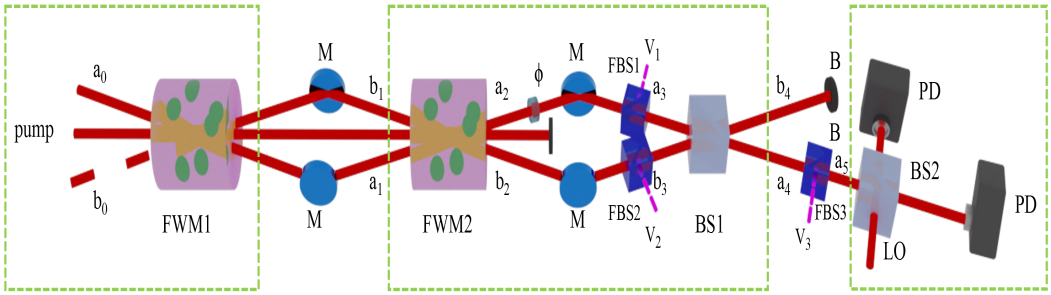

Figure 9. The device diagram of the hybrid interferometer. The other conditions are the same as those in Figure 1.

Subsequently, we discuss the phase sensitivity with different parameters. In Figure 10, the phase sensitivity versus the phase shift is displayed. In Figure 10, the HI is used to represent the phase sensitivity with the two-mode squeezed state as input via BHD based on the hybrid interferometer. In addition, the SU(1,1) in the figures represents the phase sensitivity based on the SU(1,1) interferometer with the two-mode squeezed state as input via BHD. In Figure 10a, the optimal phase sensitivities based on the HI and the SU(1,1) interferometer can beat the HL with $N = 1$, $r_1 = r_2 = 0.15$ and $r_3 = 1.5$. Our scheme demonstrates a 4% improvement in phase sensitivity compared with the HI. In Figure 10b, with $N = 100$, $r_1 = r_2 = 0.15$ and $r_3 = 1.5$, the phase sensitivity can reach the sub-SNL.

In Figure 11a, as the photon number increases, the phase sensitivities based on the HI and SU(1,1) interferometer are further enhanced. In the low-photon-number regime, both schemes can surpass the HL. And the phase sensitivity based on the SU(1,1) interferometer is always better than that of the HI. In Figure 11b,c, with lower squeezing parameters, the phase sensitivity of the SU(1,1) interferometer has better performance. With larger r_1 and r_2 values, the HI shows better phase sensitivity. According to Figure 11d, the phase sensitivity of the SU(1,1) interferometer can have the better performance when r_3 is larger than 0.04. The optimal phase sensitivity can be realized when r_3 is 0.58.

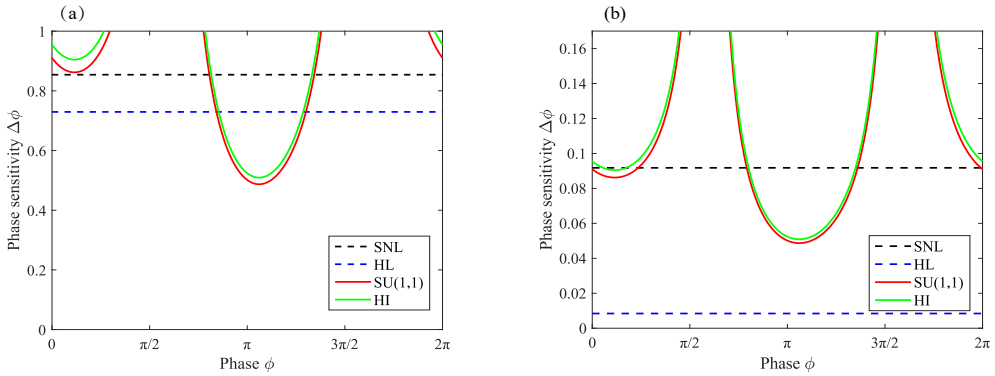

Figure 10. The phase sensitivity varies with the phase ϕ, $N = 1$ in (**a**) and $N = 100$ in (**b**) with $r_1 = r_2 = 0.15$ and $r_3 = 1.5$. HI in the figure means the phase sensitivity with BHD based on the hybrid interferometer. We use the SU(1,1) to represent the phase sensitivity with BHD based on the SU(1,1) interferometer. Here, the input state based on the HI and SU(1,1) interferometer is the two-mode squeezed coherent state. The other conditions are the same as those in Figure 3.

Next, the robustness of the two schemes against losses are indicated. With the increase in the transmission efficiency T_1, our scheme exhibits stronger robustness compared to the HI scheme, as shown in Figure 12a. When T_1 is larger than 0.41, our scheme can beat the SNL, and the HI scheme can beat SNL when $T_1 > 0.44$. In Figure 12b, it can be noted that when the transmission efficiency T_2 is higher, the phase sensitivity can always beat the HL. For the external detecting losses, our scheme exhibits stronger robustness, as Figure 12c

shows. When T_3 is larger than 0.08, the phase sensitivity of the SU(1,1) interferometer can reach the sub-SNL. For the HI scheme, the robustness is 0.5.

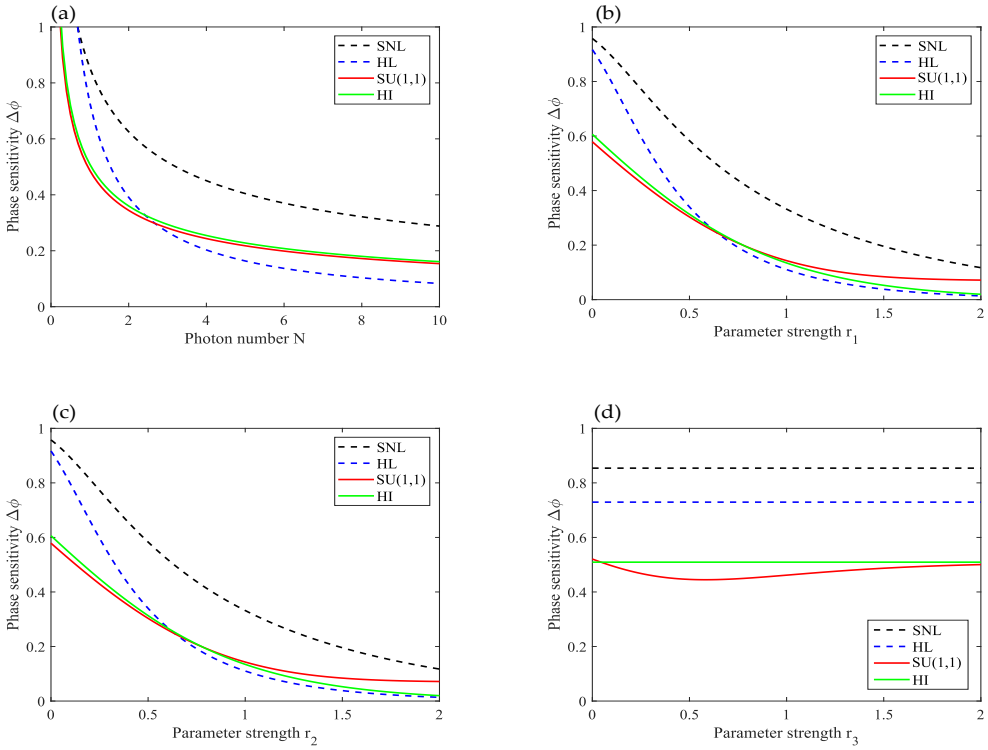

Figure 11. The phase sensitivity varies with the photon number N in (**a**) and squeezing parameter strength r_i (i = 1, 2, 3) in (**b**–**d**). $N = 1$, $r_1 = r_2 = 0.15$ and $r_3 = 1.5$. The other conditions are the same as those in Figure 10.

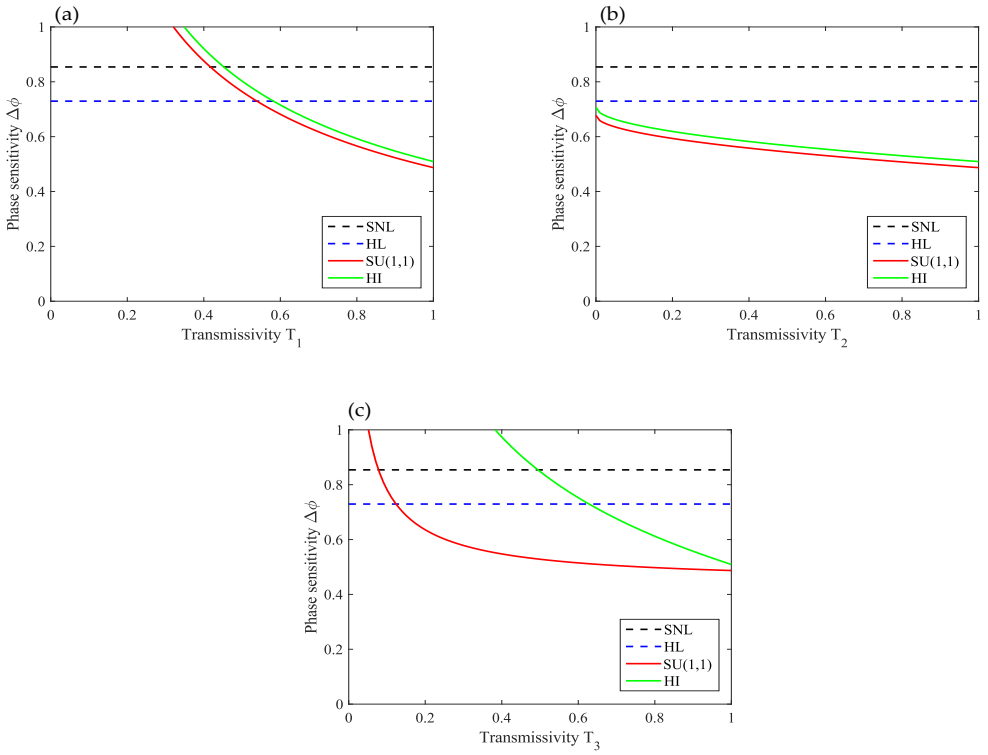

Figure 12. The phase sensitivity varies with the transmission efficiency T_i $(i = 1, 2, 3)$ in (**a**–**c**). $N = 1$, $r_1 = r_2 = 0.15$ and $r_3 = 1.5$. In (**a**), $T_2 = T_3 = 1$. In (**b**), $T_1 = T_3 = 1$. In (**c**), $T_1 = T_2 = 1$. The other conditions are the same as those in Figure 10.

7. Conclusions

In summary, we focus on the phase sensitivity of an SU(1,1) interferometer with a two-mode squeezed coherent state via BHD and ID. The QCRB can surpass the HL when the photon number is low. When the input photon number is larger, we find that the phase sensitivity with BHD can reach the sub-SNL. The optimal phase sensitivity with BHD is significantly superior to that with ID. The phase sensitivity with BHD can approach the QCRB. We also investigate the effects of internal and external losses on phase sensitivity. When the external loss reaches 10%, the optimal phase sensitivity achieved via BHD can beat the HL. The BHD has the better robustness than the ID. The external losses play a more significant role than the internal losses in our scheme. Next, we have a detailed discussion on the phase sensitivity. The optimal phase sensitivity of the proposed scheme is better than that of the HI when the input photon number is the same. In addition, our scheme has better robustness when the squeezing parameters are the same. The innovative SU(1,1) interferometer structure forms a new scheme that provides an effective approach for assessing phase sensitivity.

Author Contributions: Conceptualization, C.X. and L.W.; methodology, C.X. and S.K.; validation, C.X. and L.W.; investigation, C.X. and J.L.; writing—original draft preparation, C.X. and J.L.; writing—review and editing, C.X. and D.C. All authors have read and agreed to the published version of the manuscript.

Funding: National Natural Science Foundation of China (NSFC) under grants 12104190 and 12204312. Natural Science Foundation of Jiangsu Province BK20210874. Natural Science Foundation of Jiangxi Province 20224BAB211014 and 20232BAB201042. General project of natural science research in colleges and universities of Jiangsu Province (20KJB140008).

Data Availability Statement: All data that support the findings of this study are included within the article.

Conflicts of Interest: No potential conflicts of interest are reported by the authors.

Appendix A

In the lossy scenario, we rewrite the phase sensitivity with ID as

$$\Delta\phi_{\text{loss}} = \frac{\sqrt{\Delta^2 \hat{I}_{\text{loss}}}}{\left|\frac{\partial\langle\hat{I}\rangle}{\partial\phi}\right|_{\text{loss}}}. \tag{A1}$$

Here,

$$\begin{aligned}\Delta^2 \hat{I}_{\text{loss}} = {} & (k + T_1T_3G_3)\big(2k + 2T_3(G_3-1)+1\big)N \\ & + \big(k + T_2T_3(G_3-1)\big)\big(T_3G_3(1-T_1)+1-T_3\big) \\ & + (k + T_1T_3G_3)\big(k + T_2T_3(G_3-1)\big) \\ & + T_3(G_3-1)(1-T_2)\big(k + T_1T_3G_3 + G_3(1-T_1)+1-T_3\big),\end{aligned} \tag{A2}$$

and

$$\begin{aligned}\left|\frac{\partial\langle\hat{I}\rangle}{\partial\phi}\right|_{\text{loss}} = {} & 2T_3\sqrt{T_1T_2}\,|(2G_1-1)\sqrt{G_2G_3(G_2-1)(G_3-1)}(N+1)\sin\phi \\ & + (2G_2-1)\sqrt{G_1G_3(G_1-1)(G_3-1)}(N+1)\sin\phi|.\end{aligned} \tag{A3}$$

For the phase sensitivity with BHD, we can rewrite Equation (14) as

$$|\frac{\partial\langle\hat{X}\rangle}{\partial\phi}|_{\text{loss}} = \sqrt{T_1T_3}|\frac{\partial\langle\hat{X}\rangle}{\partial\phi}|. \tag{A4}$$

The variance can be simulated

$$\Delta^2\hat{X}_{\text{loss}} = 2k + 2T_3G_3 - 2T_3 + 1, \tag{A5}$$

where $k = m - G_3 + 1$ under the condition $T_1 = T_2 = T_3 = 1$ (ideal case). Here, $k = G_1G_2G_3(2T_1T_3 + 2T_2T_3) - 2T_2T_3G_1G_2 - G_1G_3(T_1T_3 + T_2T_3) - G_2G_3(T_1T_3 + T_2T_3) + T_2T_3G_1 + T_2T_3G_2 + 2\sqrt{G_1G_2(G_1-1)(G_2-1)}(T_1T_3G_3 + T_2T_3(G_3-1)) + 2T_3\sqrt{T_1T_2}(2G_1 - 1)\sqrt{G_2G_3(G_2-1)(G_3-1)}\cos\phi + 2T_3\sqrt{T_1T_2}(2G_2-1)\sqrt{G_1G_3(G_1-1)(G_3-1)}\cos\phi$. The phase sensitivity in a lossy scenario can be expressed as

$$\Delta\phi_{\text{loss}} = \frac{\sqrt{2k + 2T_3G_3 - 2T_3 + 1}}{|2\sqrt{T_1T_3}\sqrt{G_3}\sqrt{N}\sin(\phi+\theta_\alpha)(\sqrt{G_1}\sqrt{G_2} + \sqrt{G_2-1}\sqrt{G_1-1})|}. \tag{A6}$$

References

1. Scully, M.O.; Zubairy, M.S. *Quantum Optics*; Cambridge University Press: Cambridge, UK, 1997.
2. Dowran, M.; Kumar, A.; Lawrie, B.J.; Pooser, R.C.; Marino, A.M. Quantum-enhanced plasmonic sensing. *Optica* **2018**, *5*, 628–633. [CrossRef]
3. Taylor, M.A.; Bowen, W.P. Quantum metrology and its application in biology. *Phys. Rep.* **2016**, *615*, 1–59. [CrossRef]
4. Joo, J.; Munro, W.J.; Spiller, T.P. Quantum metrology with entangled coherent states. *Phys. Rev. Lett.* **2011**, *107*, 083601. [CrossRef] [PubMed]
5. Ma, X.P.; You, C.L.; Adhikari, S.; Matekole, E.S.; Glasser, R.T.; Lee, H.; Dowling, J.P. Sub-shot-noise-limited phase estimation via SU (1, 1) interferometer with thermal states. *Opt. Express* **2018**, *26*, 18492–18504. [CrossRef] [PubMed]
6. Gkortsilas, N.; Cooper, J.J.; Dunningham, J.A. Measuring a completely unknown phase with sub-shot-noise precision in the presence of loss. *Phys. Rev. A* **2012**, *85*, 063827. [CrossRef]
7. Aasi, J.; Abadie, J.; Abbott, B.P.; Abbott, R.; Abbott, T.D.; Abernathy, M.R.; Adams, C.; Adams, T.; Addesso, P.; Adhikari, R.X.; et al. Enhanced sensitivity of the LIGO gravitational wave detector by using squeezed states of light. *Nat. Photonics* **2013**, *7*, 613–619. [CrossRef]
8. Yurke, B.; McCall, S.L.; Klauder, J.R. SU (2) and SU (1, 1) interferometers. *Phys. Rev. A* **1986**, *33*, 4033. [CrossRef]
9. Dowling, J.P. Quantum optical metrology–the lowdown on high-NOON states. *Contemp. Phys.* **2008**, *49*, 125–143. [CrossRef]
10. Rao, Z.X.; Yang, J.W.; Liu, L.Y.; Yu, Y. High-performance NOON state from a quantum dot single photon for supersensitive optical phase measurement. *Photonics* **2024**, *11*, 512. [CrossRef]
11. Anisimov, P.M.; Raterman, G.M.; Chiruvelli, A.; Plick, W.N.; Huver, S.D.; Lee, H.; Dowling, J.P. Quantum Metrology with Two-Mode Squeezed Vacuum: Parity Detection Beats the Heisenberg Limit. *Phys. Rev. Lett.* **2010**, *104*, 103602. [CrossRef]
12. Mitchell, M.W.; Lundeen, J.S.; Steinberg, A.M. Super-resolving phase measurements with a multiphoton entangled state. *Nature* **2004**, *429*, 161–164. [CrossRef]
13. Hou, L.L.; Wang, S.; Xu, X.F. Optical enhanced interferometry with two-mode squeezed twin-Fock states and parity detection. *Chin. Phys. B* **2020**, *29*, 034203. [CrossRef]
14. Vahlbruch, H.; Mehmet, M.; Danzmann, K.; Schnabel, R. Detection of 15 dB squeezed states of light and their application for the absolute calibration of photoelectric quantum efficiency. *Phys. Rev. Lett.* **2016**, *117*, 110801. [CrossRef] [PubMed]
15. Heng, X.; Zhang, L.C.; Yin, Q.Y.; Liu, W.; Tang, L.L.; Zhai, Y.Y.; Wei, K. Quantum-Enhanced Sensing with Squeezed Light: From Fundamentals to Applications. *Appl. Sci.* **2025**, *15*, 10179. [CrossRef]
16. Jia, W.X.; Xu, V.; Kuns, K.; Nakano, M.; Barsotti, L.; Evans, M.; Mavalvala, N.; Collaboration, L.S.; Abbott, R.; Abouelfettouh, I.; et al. Squeezing the quantum noise of a gravitational-wave detector below the standard quantum limit. *Science* **2024**, *385*, 1318–1321. [CrossRef]
17. Xu, Y.K.; Chang, S.K.; Liu, C.J.; Hu, L.Y.; Liu, S.Q. Phase estimation of an SU (1, 1) interferometer with a coherent superposition squeezed vacuum in a realistic case. *Opt. Express* **2022**, *30*, 38178–38193. [CrossRef]
18. Guo, L.L.; Yu, Y.F.; Zhang, Z.M. Improving the phase sensitivity of an SU (1, 1) interferometer with photon-added squeezed vacuum light. *Opt. Express* **2018**, *26*, 29099–29109. [CrossRef]

19. Liang, X.Y.; Yu, Z.F.; Yuan, C.H.; Zhang, W.P.; Chen, L.Q. Phase sensitivity improvement in correlation-enhanced nonlinear interferometers. *Symmetry* **2022**, *14*, 2684. [CrossRef]
20. Wei, D.; Liu, J.; Yu, Y.; Wang, J.W.; Gao, H.; Li, F.L. Generation of twin Airy beams with a parametric amplifier. *J. Phys. B At. Mol. Opt. Phys.* **2015**, *48*, 245401. [CrossRef]
21. Li, D.; Yuan, C.H.; Ou, Z.Y.; Zhang, W.P. The phase sensitivity of an SU (1, 1) interferometer with coherent and squeezed-vacuum light. *New J. Phys.* **2014**, *16*, 073020. [CrossRef]
22. Ou, Z.Y. Enhancement of the phase-measurement sensitivity beyond the standard quantum limit by a nonlinear interferometer. *Phys. Rev. A* **2012**, *85*, 023815. [CrossRef]
23. Zhang, J.D.; You, C.L.; Li, C.; Wang, S. Phase sensitivity approaching the quantum Cramér-Rao bound in a modified SU (1, 1) interferometer. *Phys. Rev. A* **2021**, *103*, 032617. [CrossRef]
24. Shao, T.; Ruan, P.X.; Zhang, M.Y.; Wang, Y.X.; Zhang, M.M.; Jing, Q.L.; Liu, J. Improving phase sensitivity of a hybrid interferometer with the two-mode squeezed coherent state. *Phys. Scr.* **2024**, *99*, 105133. [CrossRef]
25. Kong, J.; Ou, Z.Y.; Zhang, W.P. Phase-measurement sensitivity beyond the standard quantum limit in an interferometer consisting of a parametric amplifier and a beam splitter. *Phys. Rev. A* **2013**, *87*, 023825. [CrossRef]
26. Manceau, M.; Leuchs, G.; Khalili, F.; Chekhova, M. Detection loss tolerant supersensitive phase measurement with an SU(1, 1) interferometer. *Phys. Rev. Lett.* **2017**, *119*, 223604. [CrossRef]
27. Xin, J. Phase sensitivity enhancement for the SU (1, 1) interferometer using photon level operations. *Opt. Express* **2021**, *29*, 43970–43984. [CrossRef]
28. Ataman, S.; Preda, A.; Ionicioiu, R. Phase sensitivity of a Mach-Zehnder interferometer with single-intensity and difference-intensity detection. *Phys. Rev. A* **2018**, *98*, 043856. [CrossRef]
29. Gong, Q.K.; Li, D.; Yuan, C.H.; Qu, Z.Y.; Zhang, W.P. Phase estimation of phase shifts in two arms for an SU (1, 1) interferometer with coherent and squeezed vacuum states. *Chin. Phys. B* **2017**, *26*, 094205. [CrossRef]
30. Shao, T.; Zhang, M.Y.; Li, C.L.; Wang, Y.X.; Hu, Y.Y.; Zhang, M.M.; Liu, J. Supersensitive phase estimation for hybrid interferometer using balanced homodyne detection. *J. Phys. B At. Mol. Opt. Phys.* **2023**, *56*, 235502. [CrossRef]
31. Jarzyna, M.; Demkowicz-Dobrzański, R. Quantum interferometry with and without an external phase reference. *Phys. Rev. A* **2012**, *85*, 011801. [CrossRef]
32. Lang, M.D.; Caves, C.M. Optimal quantum-enhanced interferometry. *Phys. Rev. A* **2014**, *90*, 025802. [CrossRef]
33. Preda, A.; Ataman, S. Phase sensitivity for an unbalanced interferometer without input phase-matching restrictions. *Phys. Rev. A* **2019**, *99*, 053810. [CrossRef]
34. Fang, Y.M.; Jing, J.T. Quantum squeezing and entanglement from a two-mode phase-sensitive amplifier via four-wave mixing in rubidium vapor. *New J. Phys.* **2015**, *17*, 023027. [CrossRef]
35. Jing, J.T.; Liu, C.J.; Zhou, Z.F.; Ou, Z.Y.; Zhang, W.P. Realization of a nonlinear interferometer with parametric amplifiers. *Appl. Phys. Lett.* **2011**, *99*, 011110. [CrossRef]
36. Li, Z.; Wang, Y.J.; Sun, H.X.; Liu, K.; Gao, J.R. Tilt measurement at the quantum Cramer–Rao bound using a higher-order hermite–Gaussian mode. *Photonics* **2023**, *10*, 584. [CrossRef]
37. Liu, J.; Shao, T.; Wang, Y.X.; Zhang, M.M.; Hu, Y.Y.; Chen, D.X.; Wei, D. Enhancement of the phase sensitivity with two-mode squeezed coherent state based on a Mach-Zehnder interferometer. *Opt. Express* **2023**, *31*, 27735–27748. [CrossRef]
38. Zhao, Z.K.; Kang, Q.Q.; Zhang, H.; Zhao, T.; Liu, C.J.; Hu, L.Y. Phase estimation via coherent and photon-catalyzed squeezed vacuum states. *Opt. Express* **2024**, *32*, 28267–28281. [CrossRef]
39. Marino, A.M.; Corzo Trejo, N.V.; Lett, P.D. Effect of losses on the performance of an SU (1, 1) interferometer. *Phys. Rev. A* **2012**, *86*, 023844. [CrossRef]
40. Yu, J.; Wu, Y.H.; Nie, L.; Zuo, X.J. High-sensitivity quantum-enhanced interferometers. *Photonics* **2023**, *10*, 749. [CrossRef]